Pergamon

Int. J. Heat Mass Transfer. Vol. 39, No. 17, pp. 3619–3632, 1996

0017-9310/96 $15.00 + 0.00

PII: S0017-9310(96)00037-3

A multiphase mixture model for multiphase, multicomponent transport in capillary porous media—II. Numerical simulation of the transport of organic compounds in the subsurface

P. CHENG and C. Y. WANG†

Department of Mechanical Engineering, University of Hawaii at Manoa, Honolulu, HI 96822, U.S.A.

(*Received* 25 *July* 1995 *and in final form* 19 *January* 1996)

Abstract—A newly developed multiphase mixture model is applied to numerically investigate infiltration and transport of nonaqueous phase liquids (NAPLs) in the unsaturated subsurface. Simultaneous flows of liquid and gas phases, solutal convection and the associated organic vapor transport in the gas phase are accounted for in the numerical model. It is shown that the numerical modeling of complex and interactive transport processes in multiphase, multicomponent systems can become computationally less intensive if based on this new model. The numerical results for three common contaminants reveal that the two-phase zone resulting from a NAPL spill is generally characterized by two distinct regions: an elongated pancake-shaped lens of high NAPL saturation which floats over the water table, and the area above it at lower saturation which was previously swept by the NAPL infiltration front. These predicted features are consistent with previous experimental observations for lighter than water NAPLs. It is also found that the vapor phase transport responsible for large-scale contamination is mainly caused by the displacement flow occurring during NAPL infiltration. In comparison, the density-driven flow due to evaporation of heavier organic chemicals is less important for systems with mobile NAPLs. Finally, several areas where future research is needed are discussed. Copyright © 1996 Elsevier Science Ltd.

1. INTRODUCTION

In a companion paper [1], a new formulation, called the multiphase mixture model, has been developed for analyzing multiphase, multicomponent transport in capillary porous media. The model is a single-domain formulation, because all the governing equations are valid throughout a problem domain encompassing various single- and multi-phase regions. In addition, the formulation strongly resembles the classical single-phase transport theory and, thus, is amenable to solutions by conventional numerical procedures. The objective of this paper is to demonstrate these salient features through application to a problem of considerable significance in the field of groundwater contamination, namely, transport of a nonaqueous phase liquid (NAPL) in the vadose zone.

Over the past decade, groundwater contamination by organic compounds such as hydrocarbon fields and halogenated organic solvents has become a major environmental concern [2]. Figure 1 schematically shows a typical contamination scenario in which an LNAPL (i.e. the NAPL is lighter than water, such as a petroleum hydrocarbon) has been released from an underground storage tank. In the unsaturated zone near the ground surface, the organic liquid as a separate phase migrates primarily downwards because gravitational forces predominate. Concurrently, the chemical volatilizes into the air in the pores, and the organic vapor is free to move laterally in the unsaturated zone, thereby greatly increasing the area of contamination. When the LNAPL reaches the saturated zone (where water completely fills the pore spaces), it will spread laterally, forming a pool or lens floating over the water table. The conceptual diagram shown in Fig. 1 indicates the two most important NAPL contamination mechanisms in the unsaturated zone, namely: (i) NAPL transport as a separate phase and (ii) organic vapor transport via gas phase advection. Modeling of these strongly coupled transport processes will ultimately determine the contaminant fate in the subsurface and subsequently identify the task of locating and removing the contaminants.

In the present paper we consider a physical problem involving simultaneous flow of a NAPL liquid and a gas phase (air). The problem is further complicated by strong interactions between the two phases through the evaporation of the organic compound into the gas phase. In the two-phase zone, the two-phase flow is driven by both capillary and gravitational forces, while in the pure gas phase region, the gas flow may be

† Author to whom correspondence should be addressed.

NOMENCLATURE

C	mass concentration of more volatile component
D	diffusion coefficient
$\boldsymbol{g}$	gravity vector
H	height of the problem domain
H_1	location of the contaminant source
H_c	length of the contaminant source
$\mathbf{j}$	diffusive mass flux
$J(s_l)$	capillary pressure function
k_r	relative permeability
K	absolute permeability
L	width of the problem domain
M	molecular weight
p	pressure
R	gas constant
s	phase saturation
t	time
T	temperature
$\mathbf{u}$	superficial or Darcian velocity vector
u	velocity component in the x-direction
v	velocity component in the y-direction
x	horizontal coordinate
y	vertical coordinate.

Greek symbols

γ	two-phase correction factor
Γ	effective diffusion coefficient
ε	porosity
λ	relative mobility
μ	viscosity
ν	kinematic viscosity
ρ	density
σ	interfacial tension.

Subscripts

air	air
c	capillary or contaminant
g	gas phase
l	liquid phase
n	normal
s	solid matrix or solutal
t	thermo-capillary
v	organic vapor
w	water
ρ	pertinent to density.

Superscripts

e	equilibrium
o	reference.

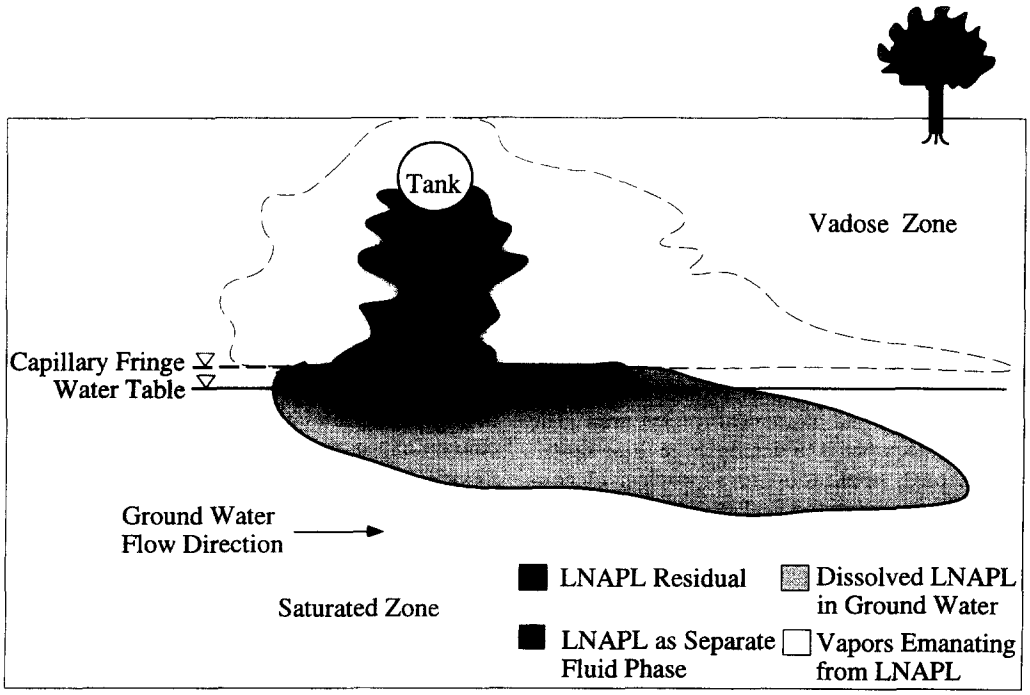

Fig. 1. Conceptual diagram of LNAPL transport in the subsurface [2].

induced by the buoyancy forces due to concentration gradients. Solutal convection is important for the transport of chemical compounds through the gas phase. Hence, the present system represents a complex two-phase, binary mixture system.

Several previous studies have been devoted to the

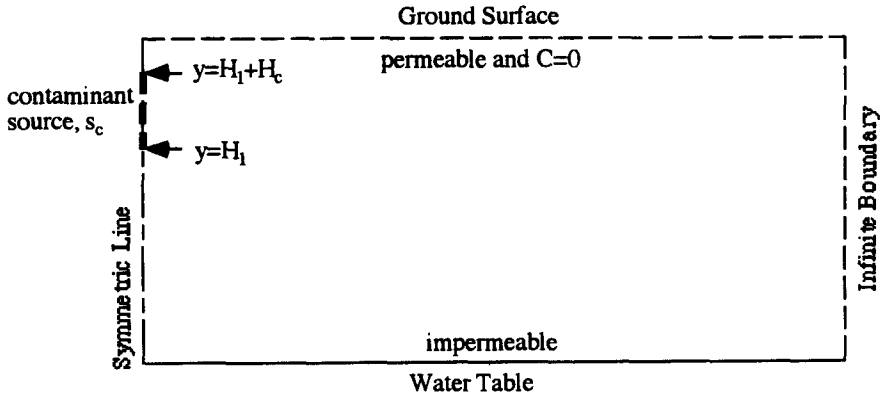

Fig. 2. Schematic of the physical problem under consideration.

topic under consideration. Pinder and Abriola [3] numerically simulated the problem using their multiphase flow formulation. Because of intensive computational efforts inherent to the formulation, the numerical results were obtained based on a rather coarse grid (i.e. 6×16). The transport of an organic compound by gas phase advection is also neglected in their work. In the more recent studies by Falta *et al.* [4] and Mendoza and Frind [5], solutally induced flow in the gas phase due to evaporation of the organic compound was found to be an important mechanism for vapor phase transport in the unsaturated zone. These studies included in-depth analyses of the gas phase transport, but assumed a stagnant NAPL, thus failing to model the NAPL infiltration process after a spill. In contrast, the present study will simultaneously account for the infiltration of the NAPL into the unsaturated subsurface and the organic vapor transport through the gas phase. Our objective is to shed light on the two important mechanisms for contaminant transport in the unsaturated zone, as well as to scrutinize the complex interactions between the two. Through such a sample application, a general solution methodology for multiphase flow and multicomponent transport problems in porous media is also established within the new theoretical framework.

2. MATHEMATICAL FORMULATION

Migration of a NAPL is considered in a two-dimensional homogeneous sand aquifer, as shown schematically in Fig. 2. The NAPL liquid is introduced into the system through a small opening of H_c in length along the left boundary, which models a contaminant source resulting from a leaky underground tank. A constant NAPL saturation is assumed to prevail inside this region during the entire infiltration process. The aquifer initially contains air and water, while the water saturation is assumed to be uniform and at a residual value; since the water phase is practically immobile ($k_{rw} = 0$) during the NAPL transport, it can be excluded from the system without much loss of generality. The system is also assumed to be isothermal at 25°C and at atmospheric pressure.

2.1. *Model equations*

A set of conservation equations governing the transport of a multiphase mixture has been developed in ref. [1]; for the system under consideration, they can be expressed as:

mass conservation

$$\varepsilon \frac{\partial \rho}{\partial t} + \nabla \cdot (\rho \mathbf{u}) = 0; \tag{1}$$

momentum conservation

$$\rho \mathbf{u} = -\frac{K}{\nu}(\nabla p - \gamma_\rho \rho \mathbf{g}); \tag{2}$$

species conservation

$$\varepsilon \frac{\partial}{\partial t}(\rho C) + \nabla \cdot (\gamma_s \rho \mathbf{u} C) = \nabla \cdot (\varepsilon \rho D \nabla C) + \nabla \cdot [\varepsilon(\rho_l s_l D_l \nabla C_l + \rho_g s_g D_g \nabla C_g - \rho D \nabla C)] - \nabla \cdot [(C_l - C_g)\mathbf{j}_l]. \tag{3}$$

In the above, the energy conservation equation has been omitted because of the isothermal condition, and the symbol C in eqn (3) denotes the mass concentration of the more volatile component, i.e. air in the present system. The mixture quantities in the above formulation are defined as

$$\rho = \rho_l s_l + \rho_g s_g \tag{4}$$

$$\rho \mathbf{u} = \rho_l \mathbf{u}_l + \rho_g \mathbf{u}_g \tag{5}$$

$$\rho C = \rho_l s_l C_l + \rho_g s_g C_g \tag{6}$$

$$\rho D = \rho_l s_l D_l + \rho_g s_g D_g \tag{7}$$

$$\nu = \frac{1}{k_{rl}/\nu_l + k_{rg}/\nu_g}. \tag{8}$$

The two correction factors γ_ρ and γ_c appearing in equations (2) and (3), respectively, are given

$$\gamma_\rho = \frac{\rho_l \lambda_l + \rho_g(1-\lambda_l)}{\rho_l s_l + \rho_g(1-s_l)} \tag{9}$$

$$\gamma_s = \frac{\rho[\lambda_l C_l + (1-\lambda_l)C_g]}{\rho_l s_l C_l + \rho_g(1-s_l)C_g}, \tag{10}$$

where the liquid mobility λ_l is

$$\lambda_l = \frac{k_{rl}/\nu_l}{k_{rl}/\nu_l + k_{rg}/\nu_g}. \tag{11}$$

Finally, the liquid diffusive flux $\mathbf{j}_l$ is expressed as

$$\mathbf{j}_l = (-\rho_l D_c \nabla s_l) + (-\rho_l D_s \nabla C) + \frac{\lambda_l(1-\lambda_l)K(\rho_l - \rho_g)}{\nu}\mathbf{g}, \tag{12}$$

where the contribution due to the temperature gradients vanishes for the present isothermal system, and the capillary diffusion and solutal-capillary diffusion coefficients are given by

$$D_c = \frac{K}{\rho_l \nu}\lambda_l(1-\lambda_l)\left[-\frac{\partial p_c}{\partial s_l}\right] \tag{13}$$

$$D_s = \frac{K}{\rho_l \nu}\lambda_l(1-\lambda_l)\left[-\frac{\partial p_c}{\partial \sigma}\frac{\partial \sigma}{\partial C}\right]. \tag{14}$$

For systems at constant temperature and pressure, the saturated vapor concentration in the two-phase zone remains nearly constant; thus, the solutal-capillary diffusion due to the concentration gradients is also absent in the present particular system (i.e. $D_s = 0$). The last term on the right hand side (RHS) of equation (12) physically implies the phase separation due to the disparate difference between the two phase densities.

In addition to the above basic conservation equations, the present formulation contains the following algebraic relations for calculating the individual phase velocities from the mixture flow field:

$$\rho_l \mathbf{u}_l = \mathbf{j}_l + \lambda_l \rho \mathbf{u} \tag{15}$$

and

$$\rho_g \mathbf{u}_g = -\mathbf{j}_l + (1-\lambda_l)\rho \mathbf{u}. \tag{16}$$

2.2. *Constitutive relations*

In this work, the relative permeabilities for the liquid and gas phases are chosen to be represented by

$$k_{rl} = s_l^3 \tag{17}$$

$$k_{rg} = (1-s_l)^3. \tag{18}$$

The two-phase capillary pressure can be expressed by a Leverett function $J(s_l)$ as follows:

$$p_c = p_g - p_l = \sigma\left(\frac{\varepsilon}{K}\right)^{1/2} J(s_l), \tag{19}$$

where

$$J(s_l) = 1.417(1-s_l) - 2.120(1-s_l)^2 + 1.263(1-s_l)^3. \tag{20}$$

As a result, the capillary diffusion coefficient given by eqn (13) can be expressed as a sole function of the liquid saturation s_l; i.e.

$$D_c = \frac{K}{\rho_l \nu}\lambda_l(1-\lambda_l)\sigma\left(\frac{\varepsilon}{K}\right)^{1.2}[-J'(s_l)]. \tag{21}$$

In the present work, the mass diffusivities of species within the liquid and gas phases are simply taken as some effective values, because a reliable model for the hydrodynamic dispersion diffusivity in a two-phase system is presently not available.

2.3. *Equilibrium phase diagram*

Closure of the system of conservation equations requires the supplementary relationships for phase saturations and mass concentrations, which are listed in Table 1.

With the assumption of local chemical equilibrium, the equilibrium air concentration in the gas phase, C_g^e, within the two-phase zone may be calculated from Dalton's law

$$C_g^e = \frac{(p-p_v)M_{air}}{p_v M_v + (p-p_v)M_{air}}, \tag{22}$$

where p_v and p are the saturated organic vapor pressure and the total gas pressure, and M_v and M_{air} are the molecular weights of the organic vapor and air, respectively. The gas phase density may be calculated from the ideal gas law

$$\rho_g = \frac{p_v M_v + (p-p_v)M_{air}}{RT} = \frac{\rho_g^o}{C_g + \frac{M_{air}}{M_v}(1-C_g)}. \tag{23}$$

The molecular weights for several common volatile organic compounds are given in Table 2, along with their saturation concentrations in the gas phase as calculated from equation (22). Compared to the dry air, all these compounds have larger molecular weights, implying that the evaporation of these organic liquids results in a gas phase density significantly larger than that of pure air and the solutally induced flows are therefore downward. The magnitude of the density-driven flow velocity in the gas phase is proportional to the density difference, $\rho_g - \rho_g^o$, and hence the ratio of molecular weights, M_v/M_{air}.

2.4. *Initial/boundary conditions*

The two-dimensional confined aquifer is assumed to be initially free of NAPL liquid and fully saturated with air, so that

$$u = v = 0 \quad \text{and} \quad C = 1 \quad \text{at } t = 0. \tag{24}$$

Table 1. Thermodynamic states in two-phase, binary systems

Conditions	$C < C_l^e(T,p)$	$C_l^e(T,p) < C < C_g^e(T,p)$	$C < C_g^e(T,p)$
Thermodynamic state	liquid	two-phase	gas
Liquid saturation, s_l	1	$\dfrac{\rho_g(C-C_g^e)}{\rho_l(C_l^e-C)+\rho_g(C-C_g^e)}$	0
Concentration in the liquid phase, C_l	C	$C_l^e(T,p)$	0
Concentration in the gas phase, C_g	0	$C_g^e(T,p)$	C

Table 2. Thermodynamic data of common groundwater contaminants at 1 atm and 25°C (the saturated vapor pressure is from Devitt *et al.* [6])

Chemical	Molecular weight, M_v, g mol^{-1}	Saturated vapor concentration, $1-C_g^e$, kg kg^{-1}
Air	28.9	—
Benzene	78.1	0.282
Carbon tetrachloride	153.8	0.487
Chlorobenzene	112.6	0.057
Chloroform	119.4	0.583
Ethylbenzene	106.2	0.049
Methylene chloride	84.9	0.800
Tetrachloroethylene	165.8	0.130
Toluene	92.1	0.110
Trichloroethylene	131.4	0.329
Xylene	106.2	0.041
1,1-dichloroethane	99.0	0.591
1,1,1-trichloroethane	133.4	0.476
1,2-dichloroethane	99.0	0.297
1,2-dichloroethylene	96.9	0.717

The ground surface at $y = H$ is permeable to the gas phase, and has a zero concentration of the organic vapor, because the concentration boundary layer above the ground surface is negligibly thin owing to a maximum rate of mass transfer to the atmosphere. Hence,

$$p = p_o \quad \text{and} \quad C = 1 \quad \text{at } y = H \quad \text{and for } t > 0. \tag{25}$$

The lower boundary is assumed to be impermeable to both phases. This boundary may represent the water table for lighter than water NAPLs or a low-permeability barrier in the case of more dense than water NAPLs. Hence,

$v = 0$ and

$$\Gamma\frac{\partial(\rho C)}{\partial y} + (C_l^e - C_g^e)\frac{\lambda_l(1-\lambda_l)(\rho_l-\rho_g)Kg}{\nu} = 0$$

at $y = 0$ and for $t > 0$, (26)

where the second condition is a concise form of the following equation reflecting no mass exchange at the water table:

$$\varepsilon\rho_l s_l D_l\frac{\partial C_l}{\partial y} + \varepsilon\rho_g s_g D_g\frac{\partial C_g}{\partial y} + (C_l^e - C_g^e)\rho_l D_c\frac{\partial s_l}{\partial y} + (C_l^e - C_g^e)\frac{\lambda_l(1-\lambda_l)(\rho_l-\rho_g)Kg}{\nu} = 0. \tag{27}$$

The first and second terms in equation (27) denote no mass transfer by diffusion through the liquid and gas phases. In practice there may be some mass transfer of organic across the water table by dissolution into the water phase, which is neglected here for simplicity. The third and fourth terms physically represent no phase migration normal to the impermeable bottom surface by capillary and gravitational forces. The first three terms describing various diffusion mechanisms can be conveniently combined into a single diffusion term appearing in equation (26), with the effective diffusivity, Γ, defined as

$$\Gamma = \begin{cases} \varepsilon D_l & \text{in the pure liquid region} \\ \dfrac{(C_l^e - C_g^e)\rho_l D_c}{\rho_l C_l^e - \rho_g C_g^e} & \text{in the two-phase zone} \\ \varepsilon D_g & \text{in the pure gas region.} \end{cases} \tag{28}$$

Using the definition of the mixture concentration, equation (6), it can be shown that equation (26) along with equation (28) is an equivalent statement to equation (27) for all regions.

The right boundary at $x = L$ is located far away from the contaminant source to approximate an infinite system. At this noncontaminated outer boundary, the air concentration in the gas phase is invariably equal to unity, and the pressure is at a static equilibrium, i.e.

$$p = p_o + \rho_g g(y - H) \quad \text{and} \quad C = 1 \quad \text{at } x = L \quad \text{and for } t > 0. \tag{29}$$

The plane at $x = 0$ is a symmetric plane so that it is impermeable to both phases, except for the contaminant source area which is permeable to the NAPL, but impermeable to the gas. The NAPL saturation in this region is assumed to be constant at s_c. Therefore

$$u_g = 0 \quad \text{and} \quad C = \frac{\rho_l s_c C_l^c + \rho_g (1 - s_c) C_g^c}{\rho_l s_c + \rho_g (1 - s_c)} \quad \text{at } x = 0 \quad \text{when} \quad H_1 \leqslant z \leqslant (H_1 + H_c) \tag{30a}$$

$$u = 0 \quad \text{and} \quad \frac{\partial C}{\partial x} = 0 \quad \text{elsewhere at } x = 0. \tag{30b}$$

3. SOLUTION METHODOLOGY AND VALIDATION

Compared to the existing multiphase formulation, the present model reduces almost by half the number of governing differential equations for the primary variables involved. Therefore, it is more suitable for numerical solutions, especially in applications where multi-dimensional effects are prominent. Secondly, each of the conservation equations in the model is similar to its counterpart in the single-phase case and, thus, many well established numerical algorithms for solving coupled single-phase transport equations can be adopted. Finally, since each of the governing equations is equally valid throughout the entire domain, explicit consideration need not be given to moving phase interfaces which separate single- from multiphase zones. Thus, the need for moving numerical grids and/or coordinate mapping is eliminated, as is the need for prescribing complex interfacial boundary conditions at internal phase interfaces. Explicit consideration is required only for boundary conditions applied to external domain surfaces.

To calculate the mixture velocity field, we follow the method proposed in Wang *et al.* [7]. The momentum equation is first substituted into the continuity equation to form the following Poisson type equation:

$$\nabla^2 p = \frac{\nu}{K}\left[\varepsilon \frac{\partial \rho}{\partial t} - \nabla p \cdot \nabla\left(\frac{K}{\nu}\right) + \nabla \cdot \left(\frac{K}{\nu} \gamma_\rho \rho \mathbf{g}\right)\right]. \tag{31}$$

In the present work, equation (31) is discretized by the central difference method and solved using the stabilized error vector propagation (EVP) method developed by Roache [8], which is a direct method for the solution of Poisson equations. The left hand side (LHS) of equation (31) is intentionally organized to have constant coefficients in order to maximize the efficiency of the EVP method. With the knowledge of the pressure field, a modified velocity field can then be calculated which is defined as

$$\mathbf{u}^* = \gamma_s \mathbf{u} = -\frac{K\gamma_s}{\mu}(\nabla p - \gamma_\rho \rho \mathbf{g}). \tag{32}$$

This modified velocity is directly usable in the species equation, equation (3). This species equation is solved by the control volume-based finite-difference formulation of Patankar [9]. The combined convective and conductive terms are discretized using the power-law scheme [9]. To obtain an interface diffusion coefficient between two control volumes, the arithmetic mean formula [9] is adopted. The equations are solved as a simultaneous set, and convergence is considered to be reached when the relative errors in the concentration and velocity fields between two consecutive iterations are less than 10^{-5}. The global mass balance is also checked and ensured to within 0.1% error after convergence is achieved.

The rectangular domain $L \times H$ is divided by a uniform and fixed grid for simplicity and for the reason that the locations of strong gradients in the primary variables are not known *a priori* and vary with time. Stringent numerical tests were performed to ensure that the solutions are independent of the grid size and time step. It was found that a 62×22 grid and a time step of 100 s generally produced sufficiently accurate results; nevertheless, all numerical results presented in this paper were obtained using an 82×32 grid and a time step of 50 s. This conservative choice of the grid size and time step was made possible because the computational effort associated with the present multiphase mixture model is relatively insignificant. A typical transient simulation (e.g. Case I in the next section) based on the 82×32 grid system and the time step of 50 s required only 2.7 CPU h of computation on an HP 715/75 workstation. In comparison, a single-phase problem with similar complexities (see below) needed the CPU time of approximately 1.8 h using the same computer code. In other words, the present computational effort for multiphase transport problems is significantly reduced and becomes comparable with those associated with single-phase convection problems. Herein lies a practical advantage offered by the multiphase mixture model developed in ref. [1].

The formulation and numerical procedures have been successfully verified through comparisons with the exact solution of McWhorter and Sunada [10] for one-dimensional horizontal air–water flow with the capillary effect taken into consideration. The capability of the numerical formulation to accommodate

density-driven flows has been verified through comparisons with the existing numerical solutions of Falta *et al.* [4] for single-phase, solutally induced natural convection in a porous medium. Qualitatively similar features have been replicated (see Section 4), although quantitative comparisons were hindered by the different coordinate systems used in the present study (i.e. the Cartesian coordinates) and in Falta *et al.* [4] (i.e. the axisymmetric coordinates). Comparison of the predictions of this study with quantitative experimental results is precluded by the paucity of such data for NAPL transport in the unsaturated subsurface. However, important physical insights have been obtained from several visualization studies [11–13], and attempts are made to insure that the predictions of this study are consistent with these previous experimental observations.

4. RESULTS AND DISCUSSION

Calculations were performed for the following three compounds that are commonly encountered in contaminated subsurfaces: carbon tetrachloride, toluene and trichloroethylene (TCE). The physical properties of these compounds are listed in Table 3 along with other information of the porous medium and contaminant source. The three chemicals selected are representative of a wide range of contaminants. As shown in Table 3, carbon tetrachloride is more dense and volatile, so that the resulting two-phase flow and gas phase advection are strong. Toluene represents an opposite case whose density is relatively low and volatilization is not great. As an intermediate case, TCE is heavier and more volatile than toluene, but is lighter and less volatile than carbon tetrachloride. For the numerical results presented below, the domain dimensions are fixed at $L = 3$ m and $H = 1$ m, which corresponds to a typical flow container for laboratory-scale experiments. The contaminant source occupies the area extending from $y = 0.6$ m to 0.8 m at $x = 0$ plane.

Emphasis of this study is placed on examining the zone contaminated by each NAPL, which is defined to encompass not only the NAPL-gas two-phase zone, but also the full gas phase region that is contaminated by the evaporated organic chemical. The contaminant volatilized into the air in the soil pores may subsequently be dissolved into flowing ground water or infiltrating recharge water, thereby contributing to contamination of the underlying ground water. Furthermore, the vapor phase transport is a key mechanism on which a popular remediation technique called soil vapor extraction is based.

4.1. *Case I: carbon tetrachloride*

Figure 3 shows the composite plots of NAPL saturation distributions in the two-phase zone and contours of constant air concentration in the pure gas phase region at times of 3, 6 and 12 h into the spill of carbon tetrachloride. The mass concentration of the organic vapor in the gas phase can be read from Fig. 3 using the conversion relation $C_v = (1 - C_g)$. Thus, the 0.99 contours shown in Fig. 3 denote 1% of organic vapor present in the gas phase, a threshold value used in the present paper to define the contamination front. The phase interface which separates the two-phase zone from the full gas phase region also represents an evaporation front at which the air concentration is constant and equal to its equilibrium value (i.e. 0.513 in the case of carbon tetrachloride at the ambient temperature). Figure 4 shows the liquid velocity vectors which are only present within the two-phase zone. The phase interface denoted by a dashed line is superimposed for a better interpretation. Figure 5 displays the gas phase velocity which decreases, by several orders of magnitude, from the two-phase zone to the full gas phase region, making it impossible to display the entire field without losing the details in the

Table 3. Thermophysical properties and other parameters used in simulations [2, 6, 14]

	Carbon tetrachloride	TCE	Toluene
Property of NAPL			
Molecular weight of contaminant, M_v [g mol^{-1}]	154	131	92
Density of the liquid phase, ρ_l [kg m^{-3}]	1584	1470	862
Dynamic viscosity of the liquid phase, μ_l [N-s m^{-2}]	9.65×10^{-4}	5.56×10^{-4}	5.52×10^{-4}
Mass diffusivity of the liquid phase, D_l [m^2 s^{-1}]	0.0	0.0	0.0
Equilibrium liquid phase concentration, C_l^e [kg kg^{-1}]	0.0	0.0	0.0
Equilibrium gas phase concentration, C_g^e [kg kg^{-1}]	0.513	0.671	0.89
Interfacial tension, σ [N m^{-1}]	0.0264	0.0284	0.028
Property of air			
Density of the gas phase, ρ_g^o [kg m^{-3}]		1.19	
Dynamic viscosity of the gas phase, μ_g [N-s m^{-2}]		1.81×10^{-5}	
Mass diffusivity of the gas phase, D_g [m^2 s^{-1}]		10^{-5}	
Molecular weight of air, M_{air} [g mol^{-1}]		28.97	
Porous medium and contaminant source			
Porosity, ε		0.4	
Permeability, K [m^2]		5×10^{-11}	
NAPL saturation in the contaminant source, s_c		0.25	

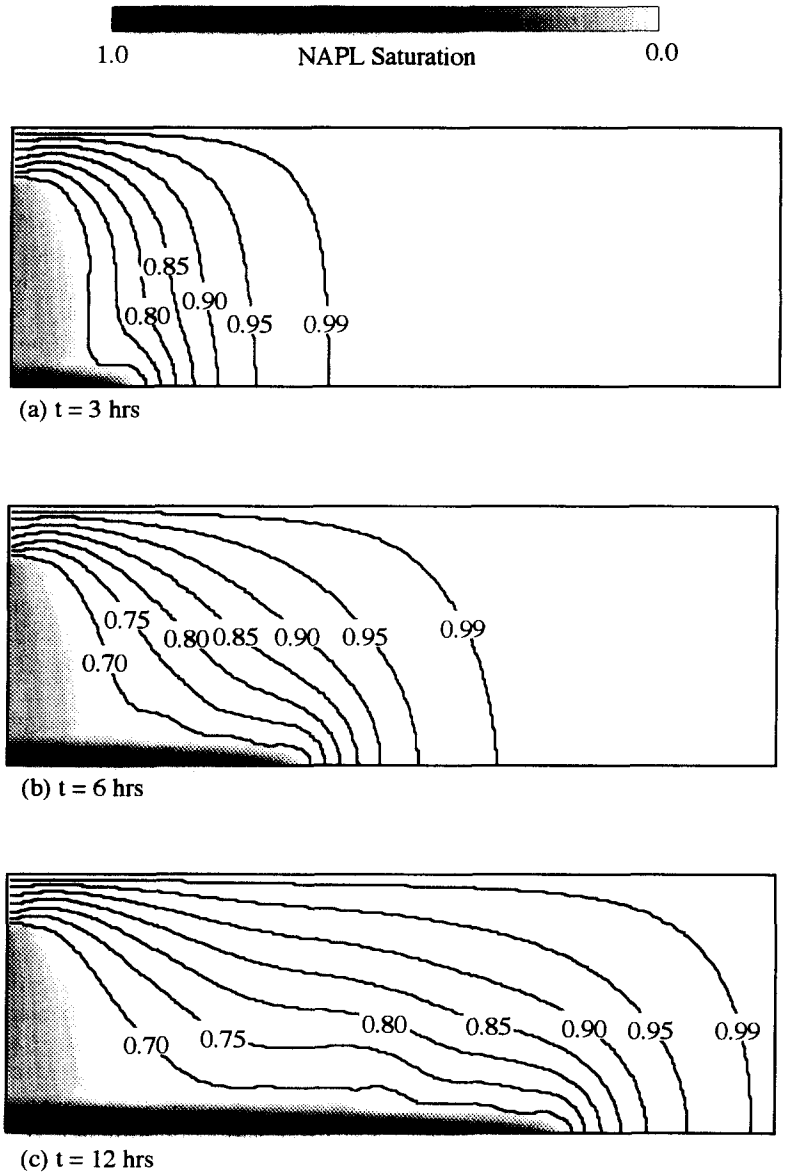

Fig. 3. Composite plots of NAPL saturation in the two-phase zone and air concentration in the gas phase for carbon tetrachloride, where $(1 - C_g)$ represents the organic vapor concentration.

pure gas phase region. In order to highlight the gas phase advection and the associated transport of organic vapors, the velocity scale shown at the bottom of each plot has been deliberately chosen to be small enough to clearly display the gas velocity vectors in the full gas phase region, as can be seen from Fig. 5, while the velocities within the two-phase zone cannot be shown because they are beyond the small velocity scale used. The NAPL saturation image is instead displayed within the two-phase zone.

At the very initial stages of NAPL invasion, a two-phase zone of a semi-circular shape develops which covers the spill spot. This is expected because the initial infiltration is governed mainly by isotropic capillary diffusion. At 3 h after the spill [Fig. 3(a)], the NAPL infiltration front reaches the bottom water table. The gravitational forces due to the disparate density difference between the NAPL and gas have dominantly controlled the two-phase flow, resulting in preferential spreading in the vertical direction than in the lateral one. This predicted shape of the NAPL infiltration front is reminiscent of the experimentally observed ones by Schwille [11] for a dense NAPL, and by Pantanzidou and Sitar [12] and Geel and Sykes [13] for light NAPLs in the unsaturated zone. The liquid phase velocity shown in Fig. 4(a) also indicates a primarily downward flow. The propagating phase interface causes a significant displacement of the gas phase, as can be seen from Fig. 5(a). The ensuing gas phase advection, in turn, spreads the volatilized organic vapor far beyond the boundary of the NAPL infiltration front [Fig. 3(a)]. The contaminant front

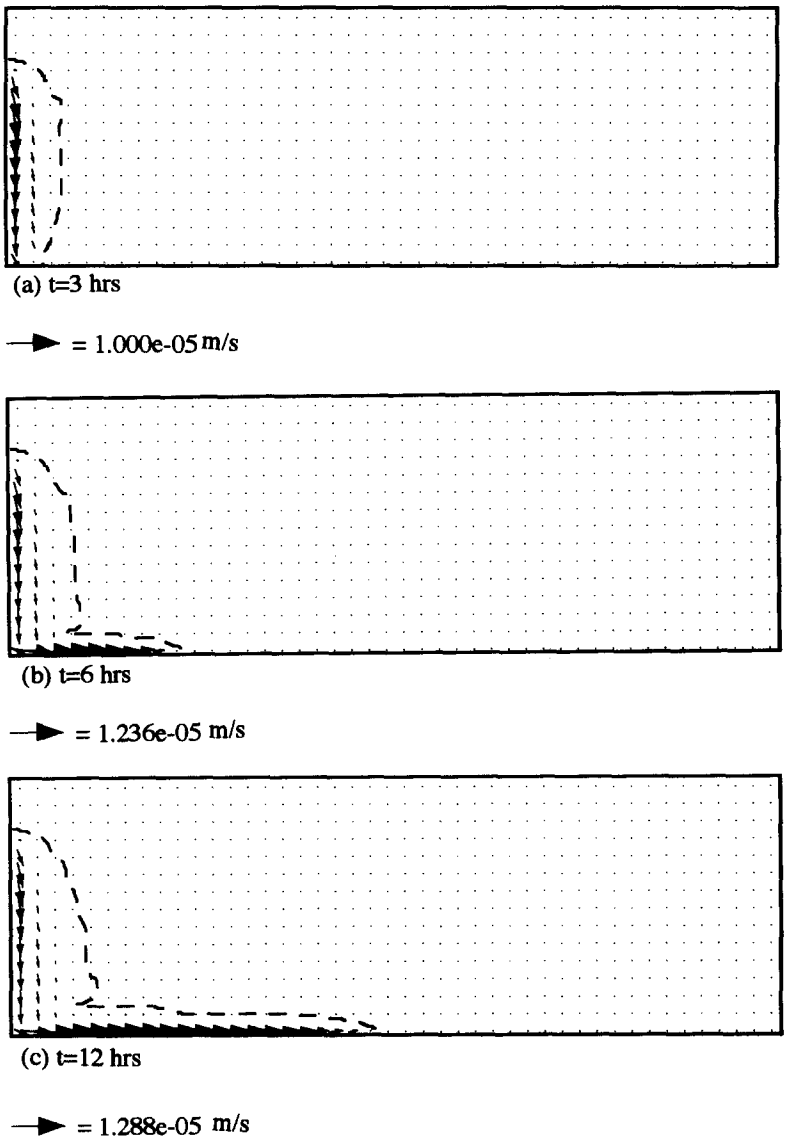

Fig. 4. Liquid velocity vector plots for carbon tetrachloride at: (a) $t = 3$ h, (b) $t = 6$ h, and (c) $t = 12$ h. The dashed line outlines the phase interface separating the two-phase zone from the full gas phase region.

denoted by the 1% contour in the organic vapor concentration is seen to penetrate into the aquifer far away from the contaminant source. It should be noted that several single-phase studies [4, 5] also indicate the wide spreading of the organic vapor by solutally induced convection. However, in the conjugate single- and two-phase flow system, the displacement flow in the gas phase caused by the propagation of the phase interface overrides the density-driven flow. The former is of the order of 3×10^{-5} m s^{-1}, as can be read in Fig. 5(a), while the latter is estimated to be only about 10^{-5} m s^{-1} ([4]; also see Fig. 6 below).

At 6 h after the spill, the phase interface motion is characterized by the horizontal migration of the NAPL along the water table at the bottom. A NAPL lens is seen to float over the water table [Fig. 3(b)], as was also observed by Pantanzidou and Sitar [12] for an LNAPL. Greater lateral spreading occurs as a result of diminishing vertical movement of the NAPL and increasingly dominant capillary forces at the leading edge of the NAPL infiltration front. The liquid velocity vector plot shown in Fig. 4(b) clearly demonstrates the horizontal flow over the water table. The moving phase interface continues to displace the gas phase [Fig. 5(b)], so that the vapor phase transport is still controlled by the displacement motion. The volatilized vapor is spread farthest at the bottom because of combined density-driven downward flow and outward flow caused by the displacement of the infiltrating NAPL [Fig. 3(b)].

By 12 h the zone of contamination has become so extensive that the contaminant front almost reaches the right boundary, which simulates an infinite boundary [Fig. 3(c)]. Hence, the simulation is terminated at

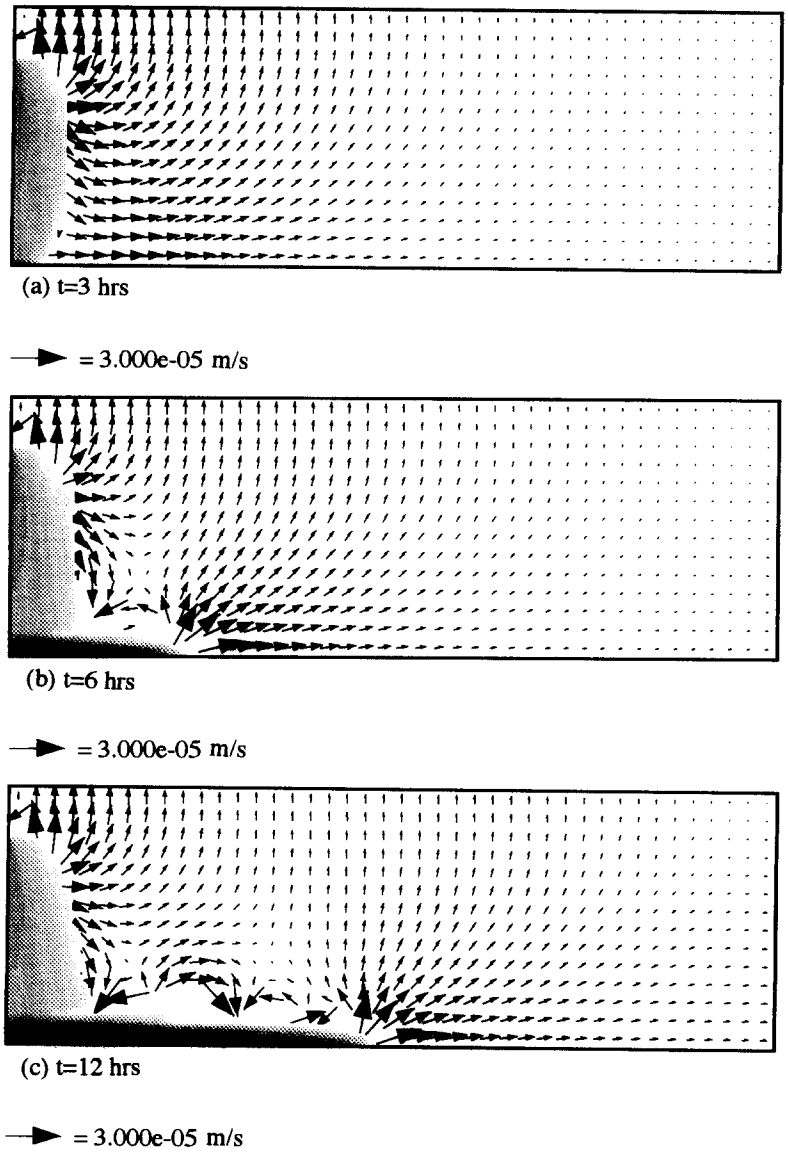

Fig. 5. Gas phase velocity vector plots for carbon tetrachloride at: (a) $t = 3$ h, (b) $t = 6$ h, and (c) $t = 12$ h. The gas phase velocities within the two-phase zone are not shown because they are beyond the scale used to highlight the gas velocity field outside the two-phase zone. The liquid saturation image is displayed instead for the two-phase zone.

this point of time. Figure 3(c) shows that the NAPL lens at the top of the water table becomes elongated and pancake-shaped, and higher NAPL saturations are found inside the lens because the NAPL is continually fed from the vertical infiltration. These predicted features are again in good agreement with the experimental observations by Pantanzidou and Sitar [12]. The fact that the NAPL saturation inside the lens can be significantly higher than that of the contaminant source is indicative of a peculiar feature of multiphase flows. That is, the gravity-induced phase separation is not a diffusion-like process and thus does not follow in the direction of the saturation gradient. The thickness of the NAPL lens depends upon the equilibrium between the gravitational and capillary forces; therefore, the thin lens predicted implies that the gravitational forces override the capillary forces in the porous medium under consideration. The gas phase velocity field is still characterized by the outward displacement due to the infiltrating NAPL. However, it can be seen from Fig. 5(c) that several small vortices develop above the NAPL lens over the water table, and these secondary flows reflect also in the fact that the concentration isopleth right next to the phase interface becomes wavy, as can be seen from Fig. 3(c). Overall, the air concentration isopleths in Fig. 3(c) indicate that the organic vapor concentrations are high near the water table. The gas of high organic vapor content combined with the direct dissolution of the NAPL lens into the water phase

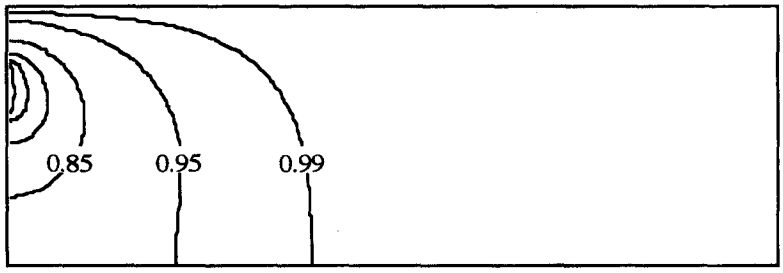

(a) air concentration (kg/kg)

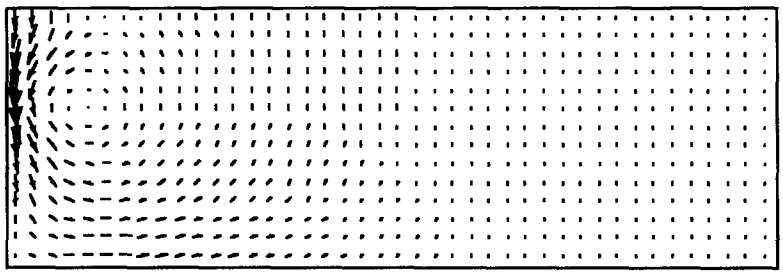

(b) gas velocity (m/s)

= 1.072e-05

Fig. 6. Plots of air concentration and gas phase velocity for an immobile carbon tetrachloride at $t = 6$ h: (a) air concentration with $(1 - C_g)$ representing the organic vapor concentration, and (b) gas phase velocity.

may cause serious contamination of the ground water system underlying the water table.

It is of interest to compare the air concentration distributions in the gas phase with and without two-phase flow. The latter situation has been extensively studied by Falta *et al.* [4] and Mendoza and Frind [5], and the importance of density-driven flow for vapor phase transport was demonstrated. However, the displacement effect caused by the presence of two-phase flow has not been included. In order to evaluate the relative importance of this displacement effect, a simulation for immobile carbon tetrachloride (i.e. the NAPL is assumed to be suspended in the pore spaces) with otherwise exactly the same conditions was carried out using the same computer code. A representative set of numerical results at 6 h is displayed in Fig. 6. As can be seen, both the air concentration isopleths and the gas velocity vectors for the immobile NAPL are very similar to those presented by Falta *et al.* [4], and Mendoza and Frind [5]. Such a comparison demonstrates the ability of the present model in successfully capturing the single-phase density-driven flow. This single-phase simulation takes about 1.8 CPU h as compared to 2.7 h for the full two-phase simulation discussed above.

Comparing the air concentration isopleths shown in Fig. 3(b) and Fig. 6(a), the difference is highly visible. The zone of contamination in the presence of two-phase flow is much more extensive than without the two-phase flow. This is not only because the NAPL migrates itself into the subsurface, but also because the displacement flow resulting from the two-phase flow greatly promotes the wide spreading of the volatilized organic vapor. In addition, the gas velocity fields are quite different in the two cases with and without two-phase flow. In the presence of two-phase flow, the gas velocity field is characterized by a displacement flow in all directions towards the permeable boundaries, while in the absence of two-phase flow, a density-driven flow towards the bottom dominates. These differences appear to indicate a need for the inclusion of NAPL movement in models of predicting gas flow and quantifying the vapor phase transport for remedial operations such as soil vapor extraction.

4.2. *Case II*: *toluene*

Toluene has a lower density than carbon tetrachloride and, therefore, a lower amount of the NAPL entering the subsurface is expected for the same saturation of the contaminant source. However, toluene is also less volatile, so that the amount of the chemical evaporated into the air in the soil pores decreases. The net effect of these counter factors results in almost the same extent of the two-phase zone, as shown in Fig. 7. Nonetheless, the full gas phase region contaminated by the organic vapor is minimal because of low volatility of toluene. Therefore, the whole zone contaminated by toluene is less extensive as compared to

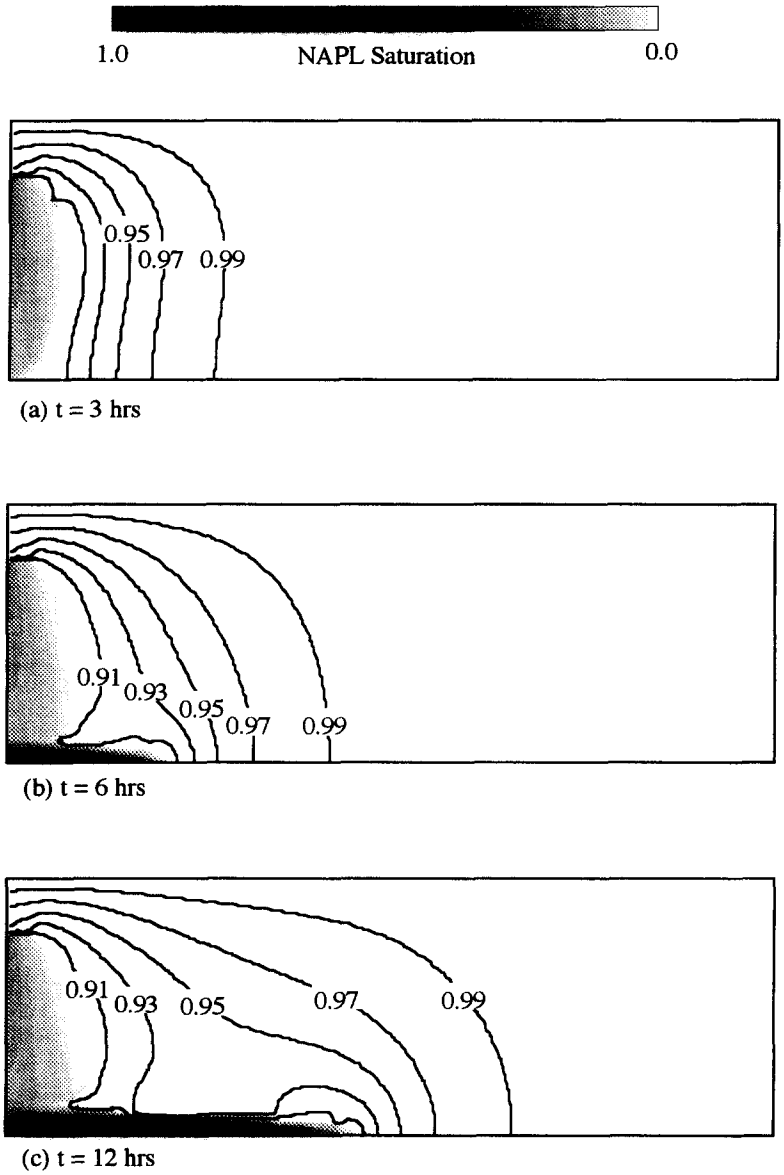

Fig. 7. Composite plots of NAPL saturation in the two-phase zone and air concentration in the gas phase for toluene, where $(1 - C_g)$ represents the organic vapor concentration.

carbon tetrachloride, provided that all other conditions are maintained the same.

4.3. *Case III*: *trichloroethylene (TCE)*

To further explore the effect of NAPL evaporation on the two-phase zone, an additional simulation using TCE as the NAPL was carried out. As seen in Table 3, TCE is as dense as carbon tetrachloride, but is less volatile. Moreover, TCE has an interfacial tension similar to carbon tetrachloride. Because the NAPL infiltration rate into the subsurface is determined mainly by the density difference between the phases and the interfacial tension, the rates for TCE and carbon tetrachloride are expected to be about the same. The two chemicals differ only in volatility, which leads to a decreasing two-phase zone in the case of carbon tetrachloride. This is indeed the case, as can be seen by comparing Fig. 8 with Fig. 3. However, the gas phase region contaminated by chemical vapor is less extensive for TCE than for carbon tetrachloride. Therefore, the whole zone of contamination remains almost the same for both TCE and carbon tetrachloride.

5. CONCLUSIONS

The multiphase mixture model developed in Part I for multiphase flow and transport in porous media has been employed to simulate the transport of non-aqueous phase liquids in the unsaturated subsurface. Two-phase flow, gas phase advection and mass transfer have been simultaneously accounted for in the

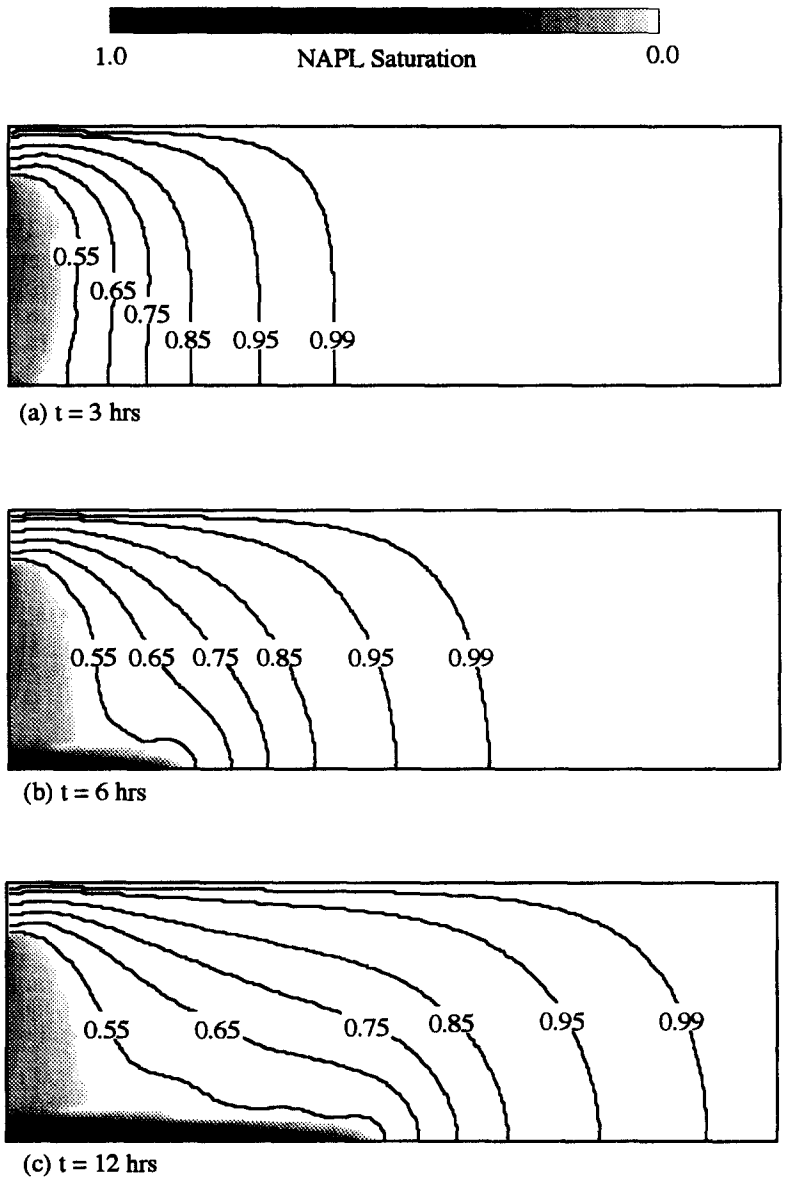

Fig. 8. Composite plots of NAPL saturation in the two-phase zone and air concentration in the gas phase for TCE, where $(1-C_g)$ represents the organic vapor concentration.

numerical simulations. It was demonstrated that using the new model, the computational effort for accurate results is affordable, even with moderate computer resources. It appears that the multiphase mixture model provides an attractive alternative for analyzing problems involving multiphase flow and multicomponent transport in porous media.

The predicted results for three representative organic compounds have revealed the complex and interactive transport phenomena occurring during NAPL infiltration. At the very initial stages of spill, the NAPL infiltration front retains a semi-circular shape, but very quickly it is characterized by more strongly vertical than lateral movement as the gravitational forces take the dominance. When the phase interface approaches the impermeable bottom boundary, the vertical movement diminishes, and the two-phase zone consists of two distinct regions: an elongated pancake-shaped lens of high NAPL saturation floating over the water table, and the area above it at lower NAPL saturation, which is previously swept by the NAPL infiltration front. These predicted results are consistent with previous experimental observations.

With regard to the vapor phase transport, high organic vapor concentrations are found near the water table. While this is partly attributed to the density-driven downward flow caused by evaporation of the organic compound, the displacement of the gas phase by the invading NAPL plays a more important role in the vapor phase transport. The wide spreading of the contaminant through this displacement mech-

anism indicates the need for a careful consideration of combined multiphase flow and vapor phase transport in the modeling of groundwater contamination systems with mobile NAPLs.

There are certainly many areas requiring future research. Experimental verification of the present predictions would establish the utility of the multiphase mixture model in a field setting, e.g. for site-specific assessment of contamination and for proposing cost-effective remediation schemes. Previous experiments [11–13] are not adequate for a full validation of the present simulations because concentration measurements in the gas phase during the NAPL infiltration were not made. The vapor phase transport, however, represents an important pathway for contaminant transport as well as a key factor to determine the feasibility of soil vapor extraction, a widely used remediation technique. Efforts are presently underway to collect comprehensive experimental data in order to provide a more complete picture of NAPL transport in the unsaturated subsurface.

In this exploratory study, several simplifying assumptions have been made. Heterogeneities (for example, zones of differing permeability) have been excluded in the numerical simulation, although the model itself is applicable to such situations. It can be expected that heterogeneities will contribute to contaminant spreading in a number of fundamental ways. For example, a NAPL tends to spread out horizontally when it encounters a low-permeability layer. In addition, the vapor phase transport becomes diffusion-dominated in low-permeability areas.

While elimination of the water phase from an actual three-phase system facilitates the numerical analysis and reduces the computational task, there remains a clear need for the modeling of a three-phase, multicomponent system in order to more thoroughly understand the NAPL transport in the realistic subsurface. A fundamentally different feature of a three-phase system is that the NAPL is no longer a wetting phase. While the NAPL can penetrate and occupy the corners of the pores in the NAPL-air two-phase system, these spaces are occupied by water in a three-phase system. Therefore, it is likely that a spilled NAPL infiltrates more rapidly in the three-phase system than in the two-phase system since all of the porosity is not available in the former to retain the NAPL at residual saturation. This phenomenon may occur despite the fact that the three-phase system offers a higher flow resistance to the NAPL infiltration.

Although the present study has demonstrated the application of the multiphase mixture model to single-component organic liquids, many groundwater pollution problems involve multicomponent organic liquids such as gasoline. When the gas phase is contaminated by multiple organic components with differing molecular diffusivities, the density-driven gas flow may become unstable and thus enhance the transport of contaminants. Under these circumstances, multi-diffusive convection occurs as a result of local buoyancy-driven instabilities formed by the difference in diffusivity of the various components. Efforts are currently underway to scrutinize these complex multicomponent systems.

Finally, the contaminant fate and transport in remediation processes is further compounded by externally-induced flow and nonisothermal conditions. For example, in the thermally-enhanced soil vapor extraction, hot air is injected into a contaminated subsurface to drive NAPLs and organic vapors into recovery wells. It is of practical interest to develop predictive capabilities for these remediation schemes based on the present multiphase mixture model.

Acknowledgements—One of us (C. Y. Wang) is grateful for support provided by a University of Hawaii seed money grant.

REFERENCES

1. C. Y. Wang and P. Cheng, A multiphase mixture model for multiphase, multicomponent transport in capillary porous media—I. Model development, *Int. J. Heat Mass Transfer* **39,** 3607–3618 (1996).
2. National Research Council, *Alternatives for Ground Water Cleanup*. National Academy Press, New York (1994).
3. G. F. Pinder and L. M. Abriola, On the simulation of nonaqueous phase organic compounds in the subsurface, *Water Resour. Res.* **22,** 109S–119S (1986).
4. R. W. Falta, I. Javandel, K. Pruess and P. A. Witherspoon, Density-driven flow of gas in the unsaturated zone due to the evaporation of volatile organic compounds, *Water Resour. Res.* **25,** 2159–2169 (1989).
5. C. A. Mendoza and E. O. Frind, Advective-dispersive transport of dense organic vapors in the unsaturated zone—2. Sensitivity analysis, *Water Resour. Res.* **26,** 388–398 (1990).
6. D. R. Devitt, R. B. Evans, W. A. Jury, T. H. Starks, B. Eklund, A. Sholsan and J. J. Van Ee, *Soil Gas Sensing for Detection and Mapping of Volatile Organics*. U.S. Environmental Protection Agency, Las Vegas (1987).
7. C. Y. Wang, C. Beckermann and C. Fan, Numerical study of boiling and natural convection in capillary porous media using the two-phase mixture model, *Numer. Heat Transfer A* **26,** 375–398 (1994).
8. P. J. Roache, *Computational Fluid Dynamics*. Hermosa, Albuquerque (1976).
9. S. V. Patankar, *Numerical Heat Transfer and Fluid Flow*. Hemisphere, Washington, DC (1980).
10. D. B. McWhorter and D. K. Sunada, Exact integral solutions for two-phase flow, *Water Resour. Res.* **26,** 399–414 (1990).
11. F. Schwille, *Dense Chlorinated Solvents in Porous and Fractured Media—Model Experiments*. Lewis Publishers, Ann Arbor (1988).
12. M. Pantanzidou and N. Sitar, Emplacement of nonaqueous liquids in the vadose zone, *Water Resour. Res.* **29,** 705–722 (1993).
13. P. J. Van Geel and J. F. Sykes, Laboratory and model simulations of a LNAPL spill in a variably-saturated sand, 1. Laboratory experiment and image analysis techniques, *J. Contaminant Hydrology* **17,** 1–25 (1994).
14. R. W. Gallant and C. L. Yaws, *Physical Properties of Hydrocarbons*. Gulf, Houston (1992).